SYNERGISTIC EFFECTS OF MINOR Be AND Zr CONTENTS ON MICROSTRUCTURAL AND MECHANICAL PROPERTIES OF A356 CAST ALLOY

O. A. B. Camargo, G. S. Padilha and F. C. Pinto
School of Applied Sciences, Research Group in Manufacturing Advanced Materials, Universidade Estadual de Campinas (UNICAMP), Limeira, SP 13484-350, Brazil

W. R. Osório and A. D. Bortolozo
School of Applied Sciences, Research Group in Manufacturing Advanced Materials, Universidade Estadual de Campinas (UNICAMP), Limeira, SP 13484-350, Brazil
School of Technology, Universidade Estadual de Campinas (UNICAMP), Limeira, SP 13484-332, Brazil

E. Poloni
Department of Materials, Centre for Advanced Structural Ceramics, Imperial College London, London SW7 2AZ, UK

https://doi.org/10.1007/s40962-024-01416-3

Abstract

The A356 aluminum alloys are largely used for manufacturing structural components in the automotive and aerospace industries due to their superior castability, strength, resistance to corrosion, and high thermal stability. This study explores for the first time the synergistic effects of minor beryllium (Be) and zirconium (Zr) additions to A356 alloys on their microstructure and mechanical properties. The alloys were solution-treated at 530 ± 2 °C and aged using T4 and T61 tempering to examine the influence of aging. The Be and Zr additions yielded significant changes in the morphology of eutectic silicon particles. Mechanical testing showed that the ultimate tensile strength (UTS) and elongation (ε) of naturally aged, T4-treated samples produced without Be and Zr increased by 20% and 47%, respectively, compared to the as-cast condition. Upon addition of Be and Zr, UTS and ε increased by 34% and 87%, reaching 243 MPa and 11% for T61 treated samples, respectively. Samples containing Be and Zr also exhibited a specific strength 10% higher and are 8% more cost-effective. The findings from this study demonstrate that A356 alloys containing minor Be and Zr additions present a promising balance of enhanced mechanical properties suitable for high-performance applications, with the potential to overcome previously reported results in similar alloys.

Received: 26 April 2024 / Accepted: 09 July 2024
Published online: 28 July 2024

Graphical Abstract

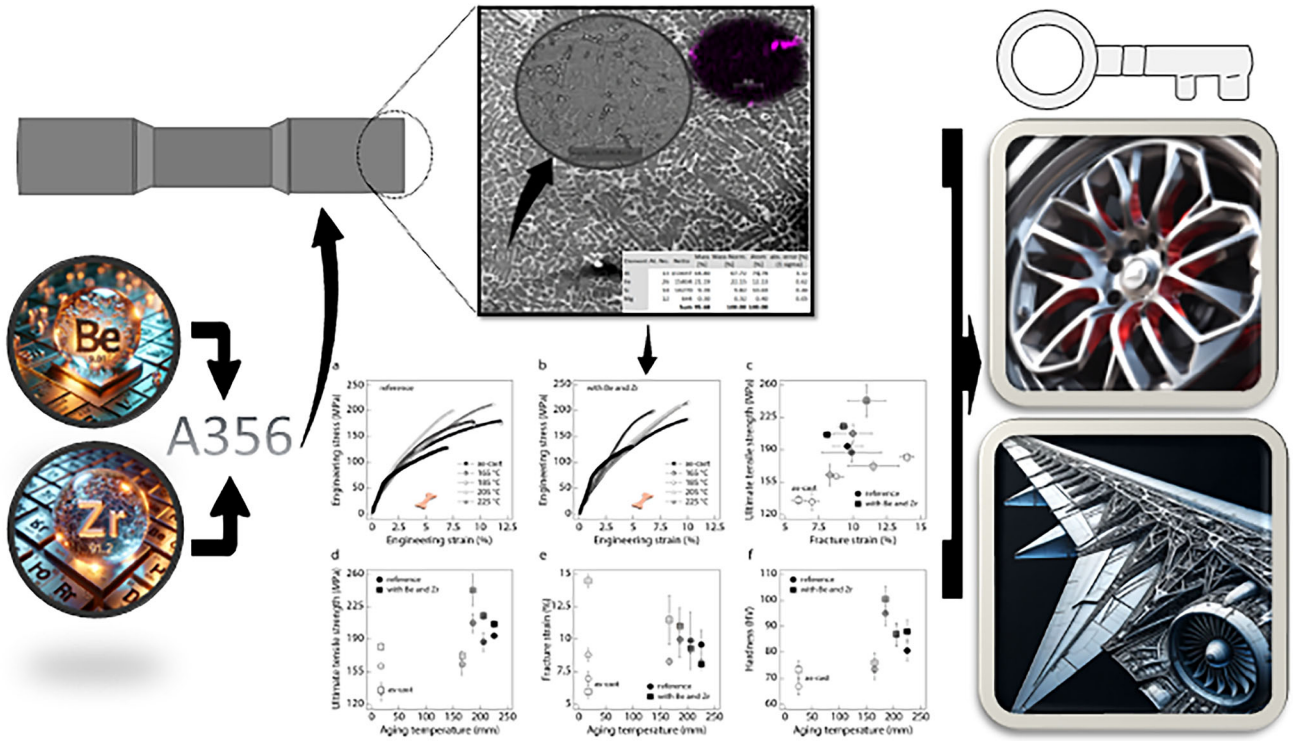

Keywords: *A356 alloy, beryllium, zirconium, master alloys, T4 and T61, microstructural and mechanical properties*

Introduction

Heat-treatable aluminum alloys are crucial in the manufacturing of structural components for the automotive and aerospace industries.[1,2] Among the wide range of aluminum alloys, the A356 type is known for its unique combination of physical and chemical properties that ensure reliable performance in demanding environments. A356 has excellent castability,[3] making it ideal for use in the manufacturing of complex parts such as engine blocks and transmission cases.[4] It is also a popular choice for wheels, gears, and structural components[4–7] due to its high strength, good ductility, and good fatigue resistance.[5] Furthermore, the A356 aluminum alloy is used in high-temperature exhaust systems and turbochargers, as it exhibits good corrosion and heat resistance.[8,9]

A356 alloys are mainly composed of aluminum, silicon, and magnesium (AlSi7Mg), and their properties are influenced by the addition of trace elements and reinforcements.[10] Notably, beryllium (Be) is added to A356 aluminum alloys to enhance their strength, stiffness, and elongation.[10–15] The Be has a higher thermodynamic drive for oxidation and nitridation than Al and Mg, which allows it to expel oxygen and nitrogen from the melt. Be atoms, being small in diameter, diffuse rapidly through the molten

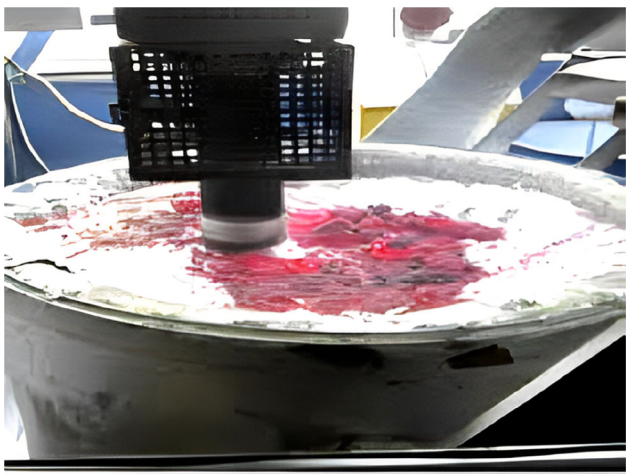

Figure 1. Representative image of the degassing process. The alloy undergoes degassing in a tundish to remove dissolved gases. Following this, the alloy is transferred to the mold using a ladle.

metal to form a thin oxide or nitride film at the melt surface. This film prevents attacks from atmospheric oxygen and nitrogen,[16,17] which is particularly important to prevent Mg to form strengthening Mg2Si precipitates and enhances precipitation kinetics.[18] Additionally, previous studies have indicated that Be addition to aluminum alloys mitigates embrittlement caused by iron intermetallics and significantly improves both strength and ductility.[11] This improvement is due to the reduction in number and size of the β-Al_5FeSi platelet-like precipitates, which are transformed into Al_8Fe_2Si with a script-like morphology.[13] Traces of Be also result in a partial modification of the eutectic Si particles in B356 and B357 alloys, similar to the effects observed with Mg addition.[14,19]

Zirconium (Zr) is another element that can be added in small amounts to A356 aluminum alloys to enhance their corrosion and heat resistance, as well as mechanical properties.[20–22] The benefits derive from the formation of fine intermetallic precipitates that inhibit recrystallization and reduce shrinkage defects.[22] Prior studies have shown that coarser Al3Zr particles dissolve into the matrix and reprecipitate as smaller particles after solution treatment at 538 °C, followed by quenching and T4 tempering, thereby increasing hardness by facilitating grain boundary movement at elevated temperatures.[22] However, the slow diffusion of Zr into Al should be avoided within the temperature range of 130–150 °C, as it can lead to the growth of Mg_2Si particles and a consequent rapid loss of hardness.[22]

Despite the clear advantages of the addition of either Be or Zr to aluminum alloys, their synergistic effect on the microstructure and mechanical properties of alloys is yet to be studied. This effect is assessed for the first time in this study by casting A356 aluminum alloys with minor amounts of Be and Zr, and by characterizing them using optical and scanning electron microscopy (SEM), energy dispersive spectroscopy (EDS), uniaxial tensile tests, and hardness measurements. The alloys are solution-treated at 530 °C for 8h and left to age naturally or artificially via T4 or T61 tempering, respectively. To achieve a balanced combination of mechanical properties, the influence of the T61 aging temperature is also analyzed.

Figure 2. Photographs of the mold and ingot. The mold is made of steel and sprayed with refractory material. The dimensions of the ingot are provided to illustrate the scale and geometry used in the experimental setup.

Experimental Procedures

Alloy Production

The samples were produced by melting about 30 kg of A356 alloy in a muffle resistance furnace, and pouring it into a rotary tundish at 450 rpm (Figure 1) under N_2 bubbling (∼ 15 L/min for 7 min).

The Al5Ti1B inoculant was applied to act as a grain refiner; while, the Al10Sr master alloy was employed to modify the morphology of the Si eutectic mixture. The goal was to achieve Ti and Sr levels of around 150 and 15 ppm, respectively, which are fractions commonly used in industry.

The Be and Zr were added to the alloy using Al–5Be and Al–10Zr master alloys, with the goal of achieving final concentrations of 100 ppm for Be and 1000 ppm for Zr. The liquid metal of samples produced with and without the addition of Be and Zr was poured into SAE 1045 permanent steel molds sprayed with refractory (based alumina powder) material (Figure 2) with dimensions 20 × 6 × 3 cm. The molds were preheated to 200 °C, and the solidification occurs naturally (air cooled).

Reference samples of A356 were labeled T. The master alloys Al5TiB and Al10Sr were added to promote grain refinement and modify the Si eutectic morphology, respectively. The samples labeled N were produced with the same alloys used in the T samples, as well as Be and Zr additives.

The examined samples were solutionized at 530 ±10 °C for 8 h, which is adopted practice in alloy manufacturing industry. Next, they were water-quenched within 10 s at 30 ± 2 °C, and pre-aged at room temperature for 24 h, a step known to achieve a balanced combination of mechanical properties.[23] Subsequently, the T and N samples were aged at temperatures of 165 ± 2 °C, 185 ± 2 °C, 205 ± 2 °C, or 225 ± 2 °C for 2.5 h and naturally cooled to room temperature. The temperature and the aging duration are two variables that define the appearance and quantity of precipitates in the matrix, with fine and dispersed morphology resulting in higher mechanical strength. In this study, we chose to keep the

aging duration constant and only vary the aging temperature. The temperature range was chosen to allow for moderate precipitation to be promoted within the matrix, as an excessive growth of precipitates could have detrimental effects on the tensile properties of the A356 alloy.

Chemical and Crystallographic Characterization

The chemical composition of the alloys was determined using optical emission spectrometry. For these analyses, the samples were polished and kept under a continuous argon flow during the test. X-ray diffraction (XRD) analysis was carried out with Cu-Kα radiation in a diffractometer using Bragg–Brentano geometry operated at 45 kV and 40 mA. The samples were scanned over a 2θ angle range of 10–120° with 15 s time intervals and a step size of 0.008°.

Macroscopic and Microscopic Characterization

For the macrostructural analysis, grinding was performed with abrasive papers with grit ranging from 320 to 1000. Subsequently, the samples were chemically etched using an aqueous solution of copper chloride (0.3 mg/mL) for an immersion time of 10 s.

For the microscopic analysis, the samples were sanded with abrasive papers from 320 to 2400 grit, rotating them by 90° after each grit change. The samples were then polished with a polishing cloth and a colloidal alumina suspension. Any remaining scratches were removed with a 9 µm diamond paste. Final chemical etching was performed for 15 s using an aqueous solution of hydrofluoric acid (0.5 vol%). Both as-cast and heat-treated samples were examined using an inverted metallographic microscope at magnifications of 100, 200, 300, 600, and 1000x. A scanning electron microscope (SEM) equipped with secondary electron and

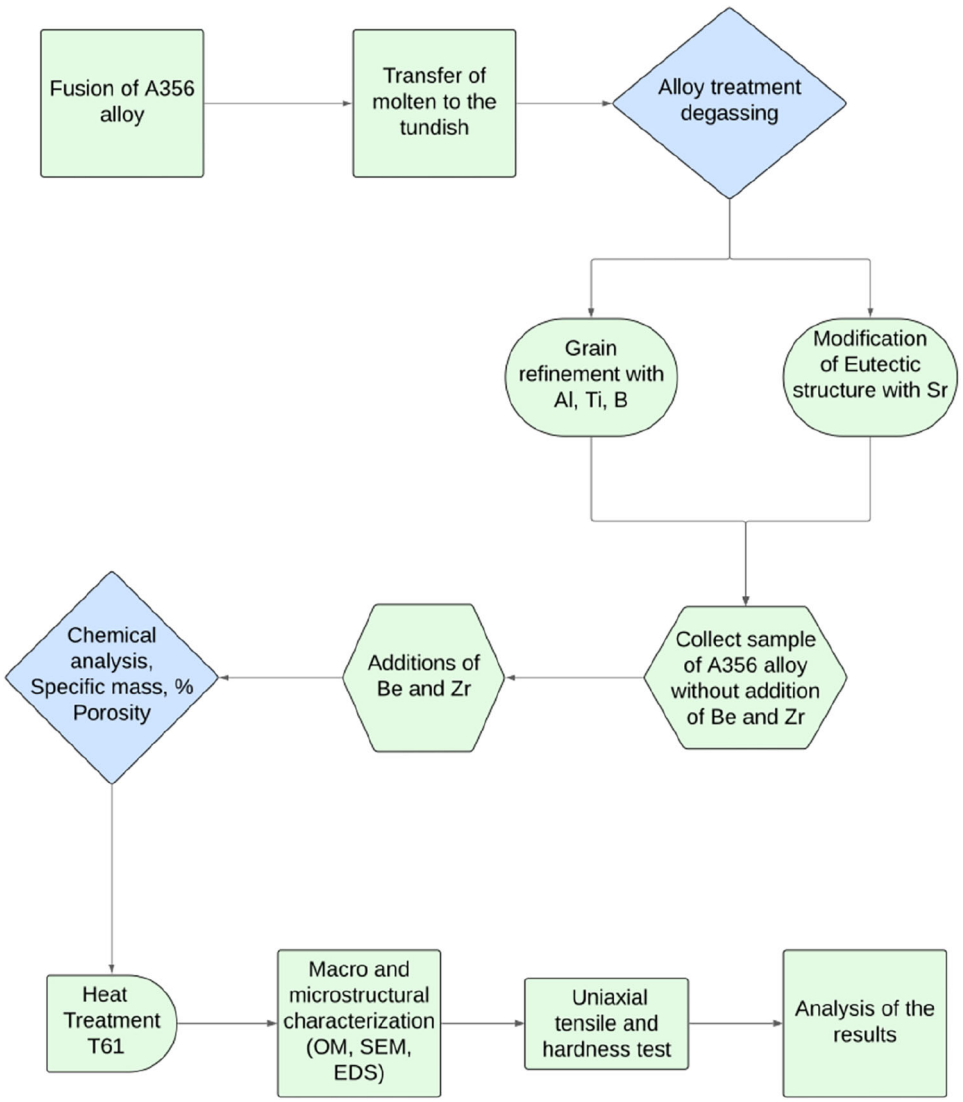

Figure 3. Process flowchart illustrating the experimental procedure for the processing and characterization of A356 alloy samples.

Table 1. Mass Fraction of Elements in A356 Alloy Samples Produced Without the Addition of Be and Zr

Samples T	Al	Si	Fe	Mg	Ti	B	Sr	Others
#1	92.5	6.9	0.142	0.256	0.121	0.0001	0.0122	Bal.
#2	92.5	6.87	0.146	0.244	0.114	0.0003	0.011	Bal.
#3	92.1	7.31	0.152	0.269	0.111	0.00076	0.0133	Bal.

These samples are labeled T.

Table 2. Mass Fraction of Elements in A356 Alloy Samples Produced With the Addition of Be and Zr (highlighted in bold)

Samples N	Al	Si	Fe	Mg	Ti	B	Sr	Be	Zr	Others
#1	92.8	6.49	0.135	0.237	0.119	0.0007	0.0099	**0.0102**	**0.114**	Bal.
#2	92.8	6.45	0.151	0.265	0.119	0.0014	0.011	**0.014**	**0.123**	Bal.
#3	92.4	6.85	0.146	0.278	0.109	0.0003	0.0116	**0.0116**	**0.079**	Bal.
#4	92.4	6.87	0.121	0.236	0.112	0.0005	0.0122	**0.011**	**0.09**	Bal.

These samples are labeled N.

Table 3. Porosity and Density Data for A356 Alloy Samples Produced With and Without the Addition of Be and Zr

	Alloy	As-cast	165 °C	185 °C	205 °C	225 °C
Density (g/cm^3)	Reference	2.648	2.627	2.636	2.634	2.637
	With Be and Zr	2.658	2.634	2.645	2.628	2.645
Porosity (%)	Reference	1.2	2.0	1.7	1.7	1.6
	With Be and Zr	0.8	1.7	1.3	2.0	1.3

backscattered electron detectors was used. The SEM was operated with a tungsten filament at 20 kV, was also utilized with a resolution of 129 eV over a 30 mm^2 area. The electron beam energy, working distance, current, and pulse count were set to 20 keV, 15 mm, 116 mA, and 60 kcps, respectively. Microstructural features such as secondary dendritic arm spacing were quantified using the free software Fiji.[24]

Mechanical Characterization

The microhardness of the samples was characterized with a Vickers indenter used with a load of 1 kgf and an indentation time of 10 s. Ten measurements, excluding the highest and lowest values, were used to calculate average values. Specimens for uniaxial tensile tests were prepared with a diameter of 6 ± 0.1 mm following the standard DIN-50125.[25] The tests were carried out at 27 ± 2 °C using a universal testing machine operated with a strain rate of 1×10^{-4} s^{-1}. The initial displacement speed was set to 0.25 mm/min until a deformation of 1 mm was reached, and to 0.5 mm/min until fracture occurred. To ensure reproducibility and determine the range of experimental errors in the obtained results, the tests were performed in triplicate.

A process flowchart is shown in Figure 3 to enhance understanding of the experimental procedures. This flowchart outlines each step of the methodology, from the initial preparation of the A356 alloy samples through to the final characterization of the material properties.

Results

Chemical Analysis, Density and Porosity

The A356 alloy samples produced with and without the addition of Be and Zr had their chemical composition, macrostructure, and microstructure characterized. The results of the optical emission spectrometry analysis of the main chemical elements in the samples are presented in Tables 1 and 2. Minor amounts of Ti and Sr were added through master alloys, as they can play a main role as a grain refiner and a eutectic modifier, respectively.

Porosity generation is linked to a range of complex factors, including the alloy's hydrogen absorption levels, inadequate interdendritic feeding, solidification range, and solid–liquid surface energies, which may decrease mechanical properties.[26] While the specific mechanism by which modifiers contribute to an increased porosity

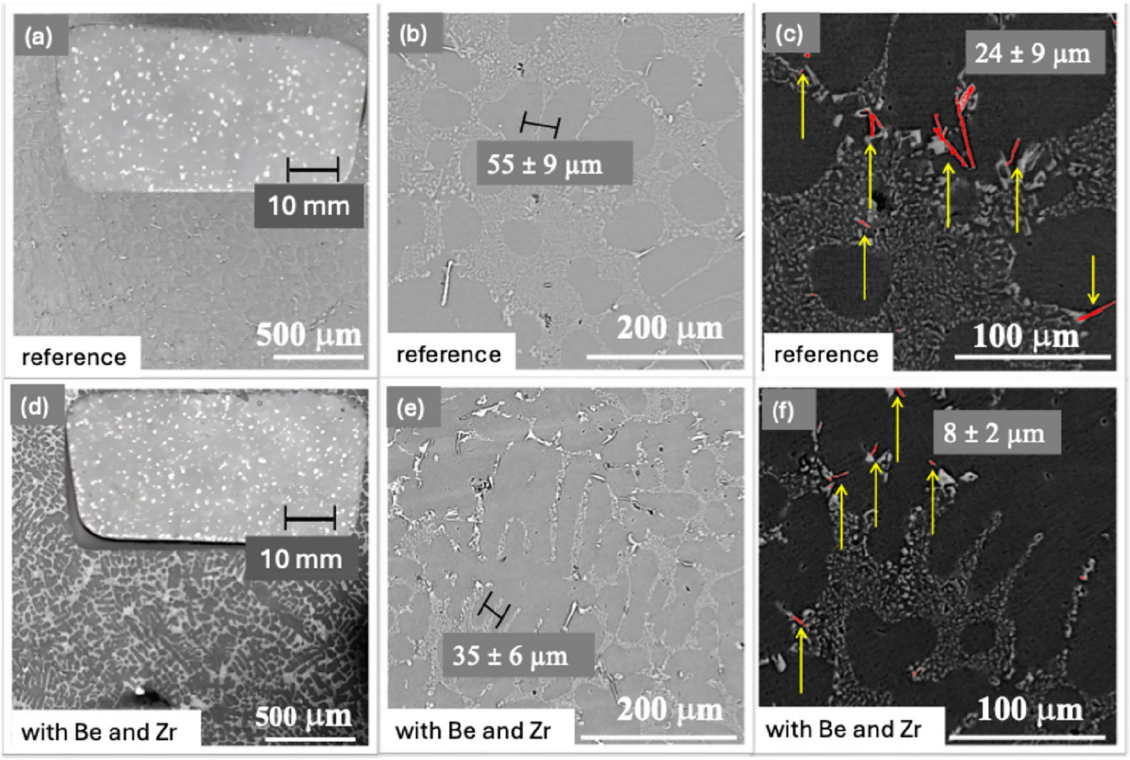

Figure 4. Microstructure of as-cast A356 alloys. (a, d) SEM images taken with a backscattered electron detector, with the macrostructure detailed in the insets. Magnified SEM images highlighting (b, e) interdendritic spacings, and (c, f) Fe-rich particles (yellow arrows). (a–c) were taken from reference samples, and (d–f) were taken from samples containing minor additions of Be and Zr.

remains debated, it is universally agreed that porosity minimization is essential.[26–28] To this end, the porosity was estimated from the density of both as-cast and heat-treated samples, as shown in Table 3.

The density measurements were conducted using Archimedes' principle, and the theoretical density of 2.705 g/cm^3 was calculated using the rule of mixtures based on the volume fractions of the most representative elements in the alloy (Al, Si, Fe, Mg, and Ti). All samples were machined from the center of the ingots, and the measurements were performed in triplicate, yielding approximate errors of 0.01 g/cm^3, 0.25% and 0.36% for density, porosity N samples and porosity T samples, respectively. The results revealed minimal porosity levels, suggesting negligible impact under the aging conditions examined.

Effect of Be and Zr on the Microstructure of A356 Alloys

Beryllium, when added to Al–Si alloys, exerts a series of beneficial effects but also has some disadvantages. Be promotes the formation of a finer microstructure,[29] which improves mechanical properties such as tensile strength and toughness. Additionally, it contributes to the formation of more stable oxides on the material's surface[30] and can influence the distribution of Si particles, increasing wear resistance. It also stabilizes beneficial intermetallic compounds such as $Al_9Fe_2Si_2$, which improves alloy homogeneity.[31] However, excessive concentrations of beryllium can lead to the formation of brittle phases in the microstructure. This can reduce ductility and increase susceptibility to fracture.[31] Similarly, Zr plays a significant role in modifying the properties of Al–Si alloys. It promotes the nucleation of fine grains during alloy solidification, resulting in a more homogeneous microstructure. Zirconium can also form thermodynamically stable intermetallic compounds with Al, such as Al_3Zr, which disperse finely in the matrix. The addition of Zr slows down the recrystallization process during heat treatments or at high temperatures.[32] Building on the reported effects obtained with the individual addition of Be and Zr, this work evaluates the synergistic effects achieved by their combined addition.

The addition of Be and Zr to as-cast A356 alloys has a visible effect on their microstructure, as shown in Figure 4. Electron microscopy and optical images of polished cross sections revealed a notable reduction in average grain size following the addition of Be and Zr (see inset on Figure 4a and d). The observed grain refinement in the as-cast structure is mainly attributed to the presence of Zr. Previous research has demonstrated that Zr enhances the formation of Al_3Zr precipitates, which play a crucial role in maintaining the stability of the microstructure. These

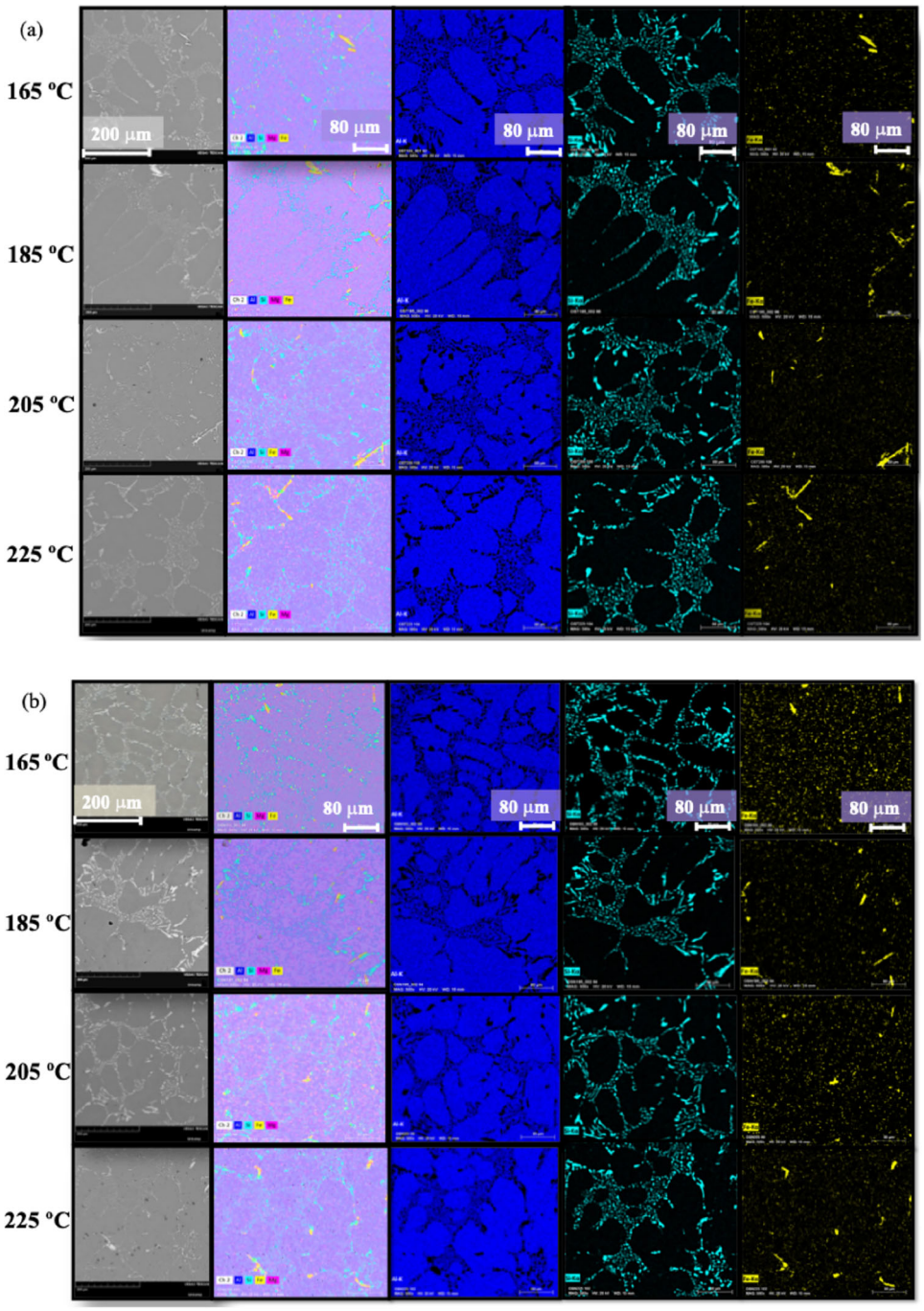

Figure 5. Micrographs of (a) T and (b) N samples after T61 heat treatment. The first column displays backscattered electron (BSE) images, providing compositional contrast. The second column presents superposed EDS element mapping, illustrating the spatial distribution of elements. The third, fourth, and fifth columns show the distribution of aluminum (Al), silicon (Si), and iron (Fe), respectively. Si and Fe-rich regions characterize the interdendritic areas.

precipitates act as locations for heterogeneous nucleation during the process of solidification, thereby enhancing strength and hardness.[20] The micrographs also reveal the presence of the well-documented Al–Si binary eutectic microstructures in both samples. The observed microstructure features a lamellar arrangement comprising α-Al dendrites within the aluminum matrix and interspersed Si-rich particles in the interdendritic regions. The identification of a Mg-rich phase (Mg_2Si), likely due to the presence of Mg (less than 0.5 wt%), is consistent with the literature.[18] Energy dispersive spectroscopy (EDS) mappings of Fe indicate the formation of AlFeSi phases.[33]

Because high cooling rates are known to enhance mechanical properties by decreasing the secondary dendrite arm spacings ($\lambda 2$),[34,35] they were not varied in this study. The $\lambda 2$ of the *T* and *N* samples were measured from the images in Figure 4b and e, respectively, yielding values of 55 ± 9 µm and 35 ± 6 µm. These values align with those reported for as-cast alloys containing refining element.[28,36] Because a similar cooling rate (approximately 1–3 °C/s) was used for all samples, the $\lambda 2$ refinement appears to be more pronounced in the N samples. This suggests that the addition of trace amounts of Be and Zr contributed to the observed microstructural refinement. Additionally, a modification in the morphology of Fe particles was observed, as highlighted in Figure 4f. The Fe intermetallics found in the T and N samples have an average length of 24 ± 9 µm and 8 ± 2 µm, respectively. Previous work by Lee et al.[11] showed that Be additions ranging from 0.04 to 0.07% changed the morphology of Fe intermetallics from large needles to equiaxed crystals. This work demonstrates that this effect can be obtained upon the addition of lower fractions of Be (approximately 0.01 wt%).

The results of the EDS analysis presented in Figure 5a and b evidence that an increase in aging temperature promotes the coalescence of Si particles. At 165 ± 2 °C and 185 ± 2 °C, the micrographs reveal the presence of fine dendritic arms. Elongated Si-rich particles and intermetallic phases can also be found near the dendrite contours. In untreated samples, the primary Si needle-like particles are typically found along the α-Al phase boundaries. Post-heat treatment, the initial and lamellar Si-rich eutectic phase transforms into fine spheroidized. Analysis of the micrographs in Figure 5 indicates that N samples T61-treated at 205 ± 2 °C and 225 ± 2 °C exhibit a more pronounced spheroidization of Si needle-like particles at the interdendritic region than samples treated at lower temperatures. The results indicate that the fibrous-like eutectic structure tends to dissolve at 205 ± 2 °C, which is evidenced by the morphological change of the Si-rich particles. The dissolution seems to be linked with the development of voids at the interdendritic boundary and adjacent to the AlFeSi particles. It is worth noting that the morphology of the AlFeSi particles remained unchanged.

The spheroidization of the Si-rich phase can be associated to the presence of Zr, eutectic modifiers such as NaF salt and Sr, and T61 treatments.[35] Zhu et al.[37] investigated the impact of T61 heat treatment on the microstructure, tensile properties, and fracture behavior of modified A356 alloys, finding that thermal treatment leads to the spheroidization of Si particles and consequently increases the ductility of the alloy.[37] Other studies have indicated that the mechanical properties of as-cast Al–Si–Mg alloys are influenced by factors such as the chemical composition, solidification conditions, morphology of silicon particles, grain refinement, and interdendritic spacing[35,38] Baradarani and Raiszadeh[22] reported the refining effect of Zr on grain size and mechanical behavior. Mahmudi et al.[39] observed mechanical property enhancements in an as-cast 319 Al alloy. Although the presence of Zr did not substantially alter dendritic spacings, a grain size reduction and an

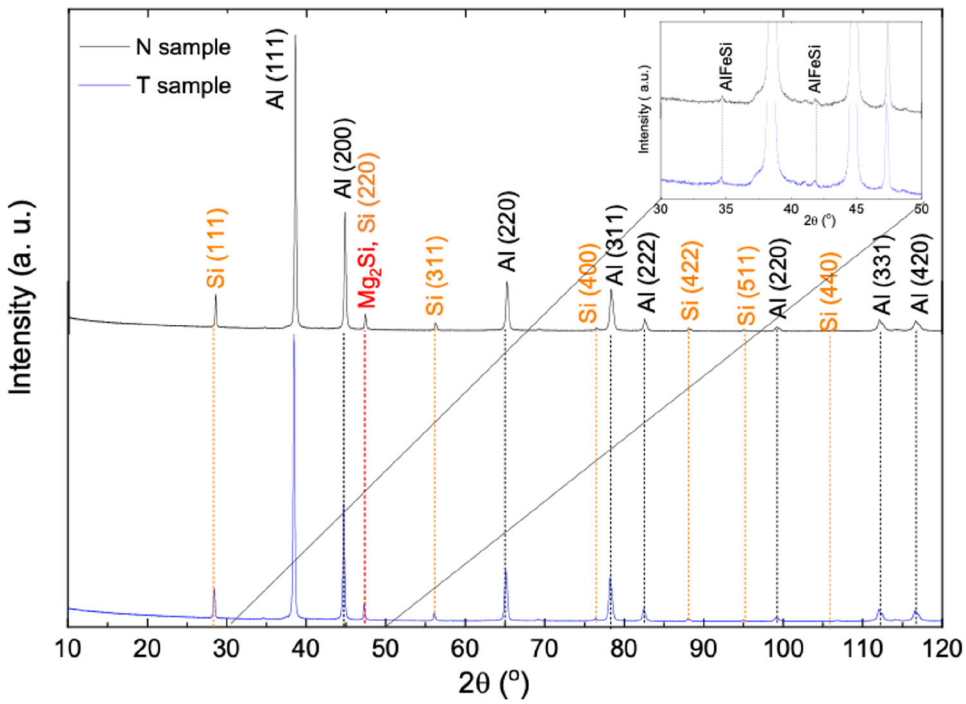

Figure 6. (a) X-ray diffraction (XRD) patterns of the examined T and N samples after T61 treatment at 185 ± 2 °C, and (b) detailed XRD ranged between 30° and 50°.

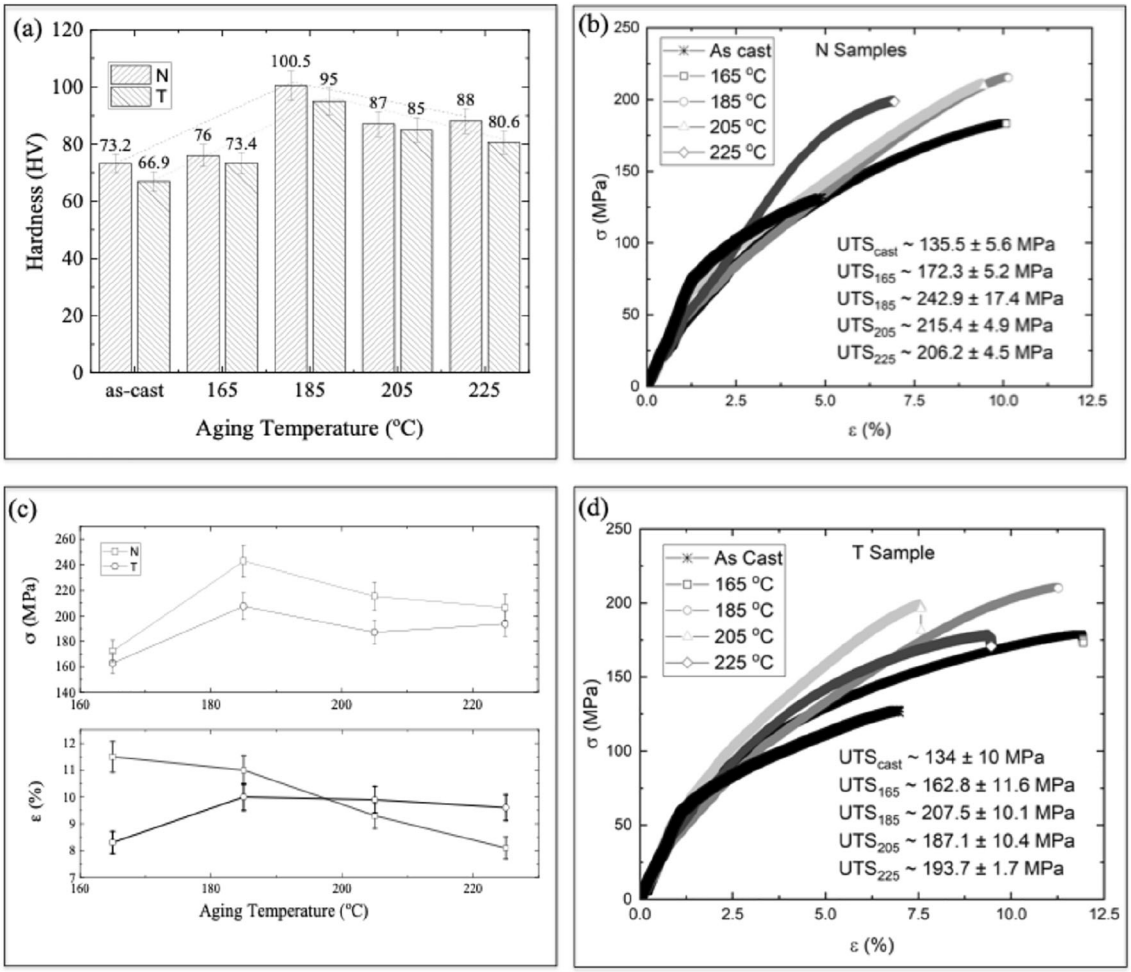

Figure 7. Experimental mechanical results for the N and T samples. (a) Hardness measurements conducted on several samples, illustrating the influence of different Be and Zr additions and heat treatment settings. (b) The stress–strain curves for the N sample demonstrate the elastic and plastic deformation zones and depicts the mechanical reaction when stress is applied. (c) The relationship between T61 heat treatment and UTS and elongation behavior is examined to illustrate the impact of thermal processing on mechanical properties, specifically strength and ductility. (d) The stress–strain curves for T samples.

increase in hardness were noted post-T61 treatment. Rakhmonov et al.[40] have demonstrated the combined effect of Zr with V and Ti on primarily grain size, also affecting the α-Al matrix. Most studies show a minor effect of Zr on grain size, but when combined with other elements, such as Cr,[41] Er,[42] and Gd,[43] the impact is notable, likely due to a low diffusion rate into the Al matrix. In this investigation, the synergistic effect of Zr and Be yielded the refinement of dendritic spacings.[41]

Additionally, the EDS results suggest that the Fe-rich phase predominantly consists of Al–Fe–Si.[38,44,45] Analyses of Fe particles at other aging temperatures yield similar results. At temperatures of 205 ± 2 °C and 225 ± 2 °C, in addition to the Al5FeSi phase, the $Al_7Si_2Fe_3$ phase is also detected. Eslsharkawi et al. showed that during solution heat treatment of 357 alloy, the disintegration of the π phase starts at certain locations where the π phase and the Al matrix meet, as well as within the π phase particles themselves. Additionally, they determined that extended periods of solution heat treatment result in a notable decrease in the proportion of the π phase, as it dissolves and decomposes into fine β phase needles.[38]

Figure 6a and b present the XRD patterns for the T and N samples following T61 treatment at 185 ± 2 °C. A detailed examination of the XRD results reveals no significant differences. Despite the inclusion of minor amounts of Mg (< 0.25) and Zr (< 0.11) in the chemical compositions (as indicated in Table 1), it appears that α- and β-AlFeSi phases and Mg_2Si[43,44] phases are not clearly present. These are identified by some low-intensity peaks. The literature[21,22,40,43] generally agrees that Zr enhances resistance to recrystallization in alloys due to the formation of Al_3Zr precipitates. Typically, fine (nanometer-scale) and metastable $L1_2$-Al_3Zr precipitates[22] are characterized using

Table 4. Experimental Results for the Ultimate Tensile Strength (UTS), Elongation (ε), Hardness, Relative Density, Relative Cost, and Specific Strength for the As-cast, and Both the T and N Samples for Different T4 and T61 Heat Treatments

Sample	Aging temperature (°C)	UTS (MPa)	ε (%)	Hardness (HV)	Relative density	Relative cost	Specific strength ($10^3 \times m^2 s^{-2}$)	
As-cast		134.0±10	6.0±1	66.9±3.3	1	1	47	55
T	165	163.0±12	8.3±0.3	73.4±3.7	0.992	1	58	66
	185	**207.5±10**	**10.0±1.4**	95.0±4.8	0.995	1	**75**	**83**
	205	187.0±10	10.0±2.2	85.0±4.3	0.995	1	67	75
	225	194.0±2	9.6±1	80.6±4.0	0.996	1	73	74
As-cast		135.5±6	7.5±1	73.2±3.2	1	1.08	47	55
N	165	172.0±5	11.5±2	76.0±3.8	0.991	1.08	63	67
	185	**243.0±17**	**11.0±1.4**	100.5±5.0	0.995	1.08	**85**	**98**
	205	215.0±5	9.3±0.4	87.0 ±4.3	0.989	1.08	80	84
	225	206.0±4.5	8.1±0.4	88.0± 4.4	0.995	1.08	76	80

Bold vlaues indicate the highest values

Transmission Electron Microscopy (TEM) or High-Resolution TEM (HRTEM) techniques. These phases, being coherent with the Al matrix, contribute to improved mechanical properties.[39]

Guo and Ohtera,[46] in their study of the Al-10Zr alloy, identified distinct Al_3Zr phases with cubic and tetragonal structures. Similarly, Liu et al.[43] reported the possible formation of an $Al_5Si_2Zr_3$ phase in Al-Si-based alloys. Regardless of the precise crystallography phase identified, Zr presence is confirmed. However, it is not possible to determine its individual impact on the microstructure conclusively.

Conversely, when XRD patterns are analyzed to identify any crystallographic configurations associated with a phase containing Be, no residual or significant peaks are detected due to the extremely low Be content. Although the addition of Be and Zr to the N sample has not yielded substantial differences in the diffractograms, a slight trend indicating a morphological transition from platelet or needle-like AlFeSi structures to Chinese script and nodular-like AlFeSi morphology can be suggested. This morphological change is more closely associated with the addition of Be, as previously reported by Lee et al.[11], Wang et al.[26], Ibrahim et al.[14], and other works.[40,41]

Mechanical Properties and their Correlations

When analyzing the hardness results of the N and T samples, no substantial differences are observed, as illustrated in Figure 7. At temperatures of 165 ± 2 °C and 185 ± 2 °C, both T and N samples exhibit an increase in hardness, followed by a downward trend as the aging temperature rises. Tash et al.[47] observed similar behavior, suggesting that a quasi-over-aging effect may occur at temperatures above 200 °C with an aging duration of 2.5 h.

Comparison of the ultimate tensile strengths and hardness values between the N and T samples shows trends to support the N sample, as also depicted in Figure 7. Similarly, the trend in elongation is upward. The addition of Be and Zr has resulted in increases in deformation by 21%, 15%, 14.4%, and 24.5% at aging temperatures of 165 ± 2 °C, 185 ± 2 °C, 205 ± 2 °C, and 225 ± 2 °C, respectively.

With approximately 1100 ppm Zr and 100 ppm Be used in the experiments, good mechanical improvements are achieved. For instance, comparing the as-cast sample with the aged samples at 185 ± 2 °C, the UTS has increased to approximately 120 MPa (a ∼ 50% increase). Ibrahim et al.[14] reported a similar enhancement, attributing the UTS improvement to Be's role in increasing the precipitation of the hardening Mg_2Si phase and preventing the oxidation of Mg and Zr, thus refining the grain.[14]

Chen et al.[48] reported very similar UTS and elongation results for an Al–Si–Mg alloy (labeled ZL104) with slightly higher Si content (∼ 8 wt% Si) and a similar level of Mg (∼ 0.2 wt% Mg), achieving a UTS of 243 MPa and elongation of 12%. However, the Al–Si alloy in their study had a higher Si content and underwent squeezed casting. They evaluated a flywheel housing part weighing approximately 20 kg and applied a solution treatment at 550 °C for 3 h, showing an increase in UTS to ∼ 300 MPa after aging at 175 °C for 8 h. While direct comparisons between different studies can be challenging, it is evident that the minor Be and Zr additions to the A356 alloy in this investigation represent a competitive approach for various applications.

Table 4 summarizes the obtained UTS results, elongation, hardness, relative density, relative cost, and specific strength for all samples tested. The highlighted values correspond to the best performances achieved. The data in Table 4 suggest that quenching followed by pre-aging for 24 h enhances both N and T samples, resulting in UTS increases of about 20% and 35%, respectively, while deformations increase by approximately 1.5 and 2.3 times compared to the as-cast condition. This leads to two conclusions about the strengthening mechanism: first, even without the addition of minor Be and Zr and only with pre-aging (T4 for 24 h), both UTS and deformation increase by ~ 20%, from 135 MPa for as-cast to 161 MPa for pre-aged condition. Second, the improvements in both UTS and deformation are further enhanced by ~ 35% when Be and Zr are added, rising from 135 to 182 MPa.

Additionally, the T sample achieves the best UTS results when aged at 185 °C, which correlates with optimal UTS and deformation. Focusing only on UTS values, samples aged at 185 °C yield the most favorable outcomes, despite a marginally increased density.

The behavior observed, where a mechanical parameter, such as UTS or hardness, reaches a maximum value and then shows a slight decreasing trend or plateaus with increasing aging temperature or time, is also noted in other Al–Si-based alloys.[20,39] This phenomenon is attributed to 'over-aging,' as reported by Baradarani and Raiszadeh[22] and Mahmudi et al.[39]

When specific strength values are calculated, the highest specific strength values correspond to samples treated at 185 °C. Notably, the N sample, which contains minor Be and Zr contents, exhibits values of specific strength up to 20% higher than the T sample, ranging from 85 to 98 × 10^3 m^2 s^{-2} compared to 75 to 83 × 10^3 m^2 s^{-2}. These findings are significant even when relative costs are considered, which were calculated based on the added percentages of Zr and Be.

Furthermore, the extent of deformation observed in the N samples is noteworthy. While an aging temperature above 185 °C appears to have a detrimental effect on UTS and deformation in the T samples. In terms of the specific strength, the N sample aged at 185 °C exhibits a UTS nearly twice as high as that of the as-cast sample. This indicates that aging and the addition of Be and Zr can offer competitive advantages, even though the energy consumption values for the treatment have not been directly calculated.

Interestingly, high ε levels were obtained in this study. When comparing the UTS of both the N and T samples with results previously reported in the literature,[48–51] it is evident that the elongation levels for both sample types are significant. While similar or higher UTS levels have been reported (up to 300 MPa), the elongation observed here is considerably greater than those earlier findings.[49] As reported by Dash and Chen,[49] a variety of Al–Si-based alloys, produced through different manufacturing processes, have been cataloged. Specifically, A356 alloys (or equivalents) produced via conventional casting and subjected to T61 treatment exhibit UTS and ε of approximately 260 MPa and 5%[50]; another study reports 273 MPa and 3.5%.[51] This underscores that the ε levels attained in the current investigation are noteworthy, reaching up to 14%.

To discern which parameters most significantly influence this elongation, both the treatments applied, and the minor elements added have been scrutinized. For the T samples treated with both T4 and T61 processes, the ε levels across the samples show no significant variation. Conversely, for the N samples the most pronounced ε levels (approximately 14%) correspond to the T4 treatment, markedly surpassing those previously reported.[49–51]

However, an increase in aging temperature has a varied effect. Unlike the T samples, where ε remains consistent, the N samples exhibit a pronounced decrease in ε under T61 treatment, indicating a deleterious effect. This suggests that the choice between T4 and T61 treatments, in relation to the desired balance of tensile strength and deformation, must be carefully considered. Therefore, if the goal is to achieve maximum ultimate tensile strength, a T61 treatment at 185 °C with the addition of minor Be and Zr contents is recommended. Alternatively, for designs where elongation is a priority, while still requiring reasonable tensile strength, employing only T4 treatment with Be and Zr additions is advisable. Furthermore, for applications where specific strength is of utmost importance, the values presented in Table 3 should be referenced.

Conclusions

Based on the results obtained for as-cast and T4 and T61 treated samples produced without (T samples) and with (N samples) minor fractions of Be and Zr, the following conclusions can be drawn:

- Both T and N samples showed eutectic structural changes. The inclusion of Sr results in a 50% decrease in secondary dendrite arm spacings (from ~ 60 to ~ 30 μm) in samples with Be and Zr. AlFeSi morphology changes from platelet or needle-like to nodular or script-like, mostly due to Be. Adding Be and Zr refines the microstructure. All samples had comparable X-ray diffractograms, confirming that the reported modifications are not crystallographic.
- The T and N samples showed significant differences in mechanical characteristics. The T samples

aged naturally (T4 treatment for 24 h) had 20% higher UTS and 47% higher ε values than as-cast samples. Naturally aged N samples showed 34% and 87% increases in UTS and ε. These results demonstrate that modified alloys can be used in high-performance applications since they perform similarly or better than previous research.

- The N samples show considerable elongation of 14% after T4 treatment, compared to other samples and earlier investigations. The T61 treatments at different temperatures reduced elongation in these samples. Elongation dropped to 8% after T61 treatment at 225 °C. This number is equivalent or better than earlier studies.
- Beryllium and Zr additions resulted in N samples outperforming T samples in UTS and specific strength by 10% across all T4 and T61 heat treatments. The UTS and specific strength of N samples were maximized after T61 treatment at 185 °C, although elongation was highest after T4. In some projects and applications, the T4 versus T61 trade-off between mechanical strength and elongation is critical. With Be and Zr, the cost rises by 8% economically.

The authors would like to emphasize that implementing safe handling practices, including the use of personal protective equipment and emissions control measures such as adequate ventilation systems, is essential to mitigate the health risks posed by beryllium toxicity in the workplace and to ensure the well-being of workers.

Acknowledgements

The authors acknowledge Mr. Luiz A. Garcia for his contributions to technical aspects and equipment organization. This work had the financial support of FAEPEX-UNICAMP (Grants #2252/23 and #2259/19), the Coordination for the Improvement of Higher Education Personnel (CAPES, Ministry of Education, Brazil), the National Council of Scientific and Technological Development (CNPq, Grants #310010/2020-9, #407595/2022-8, #313272/2021-2 and #305207/2023-7) and the São Paulo Research Foundation (FAPESP, Grants #2016/13352–0, and #2013/12729–5).

REFERENCES

1. P. Rambabu, N. Eswara Prasad, V.V. Kutumbarao, R.J.H. Wanhill, Aluminium alloys for aerospace applications. *Aerospace Materials and Material Technologies: Volume 1: Aerospace Materials*, pp. 29–52 (2017)
2. D. Ashkenazi, How aluminum changed the world: a metallurgical revolution through technological and cultural perspectives. Technol. Forecast. Soc. Change **143**, 101–113 (2019)
3. K.R. Ravi, R.M. Pillai, K.R. Amaranathan, B.C. Pai, M. Chakraborty, Fluidity of aluminum alloys and composites: a review. J. Alloys Compd. **456**, 201–210 (2008)
4. T. Alam, A.H. Ansari, Review on aluminium and its alloys for automotive applications. Int. J. Adv. Technol. Eng. Sci **5**, 278–294 (2017)
5. S.J.S. Chelladurai et al., A review on mechanical properties and wear behaviour of aluminium based metal matrix composites. Mater. Today Proc. **37**, 908–916 (2021)
6. J. Ou et al., Advanced process simulation of low pressure die cast A356 aluminum automotive wheels—part I, process characterization. Metals (Basel) **10**, 563 (2020)
7. G. Niu, Y. Wang, L. Zhu, J. Ye, J. Mao, Fluidity of casting Al–Si series alloys for automotive lightweighting: a systematic review. Mater. Sci. Technol. **38**, 902–911 (2022)
8. M.N. Sanath, C.L. Nihal, P.M. Shivaprasad, H.V. Puneeth, M.K. Srinath, Review on corrosion studies of heat treated Al–Si alloy. in *IOP Conference Series: Materials Science and Engineering*, vol. 1258, p. 012028 (IOP Publishing, 2022)
9. N.S. Ebenezer et al., Experimental studies on damping behaviour of nickel electroplated A356.2 alloy. Mater. Today Proc. **27**, 1038–1044 (2020)
10. T.H. Ludwig, P.L. Schaffer, L. Arnberg, Influence of some trace elements on solidification path and microstructure of Al–Si foundry alloys. Metall. Mater. Trans. A **44**, 3783–3796 (2013)
11. J.-K. Lee, M.-H. Kim, S.-H. Choi, Beryllium effects on the microstructure and mechanical properties of A356 aluminium casting alloy. J. Korea Foundry Soc. **18**, 431–438 (1998)
12. O. Janka, R. Pöttgen, The role of beryllium in alloys, Zintl phases and intermetallic compounds. Zeitschrift für Naturforschung B **75**, 421–439 (2020)
13. P.-S. Wang, S.-L. Lee, J.-C. Lin, M.-T. Jahn, Effects of solution temperature on mechanical properties of 3190 aluminum casting alloys containing trace beryllium. J. Mater. Res. **15**, 2027–2035 (2000)
14. M.F. Ibrahim, S.A. Alkahtani, K.A. Abuhasel, F.H. Samuel, Microstructural characterization of beryllium treated Al–Si alloys. Adv. Mater. Sci. Eng. **2015**, 673025 (2015)
15. E.A. Elsharkawi, M.F. Ibrahim, A.M. Samuel, H.W. Doty, F.H. Samuel, Understanding the effect of Be addition on the microstructure and tensile properties of Al–Si–Mg cast alloys. Int. J. Metalcast. **16**, 1777–1795 (2022). https://doi.org/10.1007/s40962-021-00715-3
16. A. Dehhaghi, S.M.A. Boutorabi, Nano double oxide film (NDOF) characteristics of A356 alloy casting protected with beryllium in turbulence conditions. Found. Res. J. **2**, 71–78 (2018)

17. N. Smith, A. Kvithyld, G. Tranell, The mechanism behind the oxidation protection of high Mg Al alloys with beryllium. Metall. Mater. Trans. B **49**, 2846–2857 (2018)
18. G. Asghar, L. Peng, P. Fu, L. Yuan, Y. Liu, Role of Mg_2Si precipitates size in determining the ductility of A357 cast alloy. Mater. Des. **186**, 108280 (2020)
19. M.A. Moustafa, F.H. Samuel, H.W. Doty, S. Valtierra, Effect of Mg and Cu additions on the microstructural characteristics and tensile properties of Sr-modified Al–Si eutectic alloys. Int. J. Cast Met. Res. **14**, 235–253 (2002)
20. M.H. Abdelaziz, A.M. Samuel, H.W. Doty, F.H. Samuel, Effect of morphological changes of eutectic Si particles on the ambient and high temperature tensile properties of Zr containing Al–Si alloys. J. Market. Res. **9**, 5962–5981 (2020)
21. H. Huang, C. Hu, D. Song, Z. Jia, N. Zhou, Microstructure characteristics and elevated-temperature tensile properties of Al-7Si-0.3 Mg alloys with Zr and Hf addition. J. Mater. Eng. Perform. **30**, 9059–9066 (2021)
22. B. Baradarani, R. Raiszadeh, Precipitation hardening of cast Zr-containing A356 aluminium alloy. Mater. Des. **32**, 935–940 (2011)
23. D. Apelian, S. Shivkumar, G. Sigworth, Fundamental aspects of heat treatment of cast Al–Si–Mg alloys. AFS Trans. **97**, 727–742 (1989)
24. J. Schindelin et al., Fiji: an open-source platform for biological-image analysis. Nat. Methods **9**, 676–682 (2012)
25. N.N. DIN, 50125-Testing of metallic materials-Tensile test pieces. Preprint at (2009)
26. Q. Wang, Q. Hao, W. Yu, Effect of strontium modification on porosity formation in A356 alloy. Int. J. Metalcast. **13**, 944–952 (2019)
27. C.M. Dinnis, A.K. Dahle, J.A. Taylor, M.O. Otte, The influence of strontium on porosity formation in Al–Si alloys. Metall. Mater. Trans. A **35**, 3531–3541 (2004)
28. H.R. Ammar, A.M. Samuel, F.H. Samuel, Porosity and the fatigue behavior of hypoeutectic and hypereutectic aluminum–silicon casting alloys. Int. J. Fatigue **30**, 1024–1035 (2008)
29. M. Rejaeian, M. Karamouz, M. Emamy, M. Hajizamani, Effects of Be additions on microstructure, hardness and tensile properties of A380 aluminum alloy. Trans. Nonferrous Metals Soc. China **25**, 3539–3545 (2015)
30. O.O. Joseph et al., Effects of alloying on aluminium-silicon alloys–a review. in *IOP Conference Series: Materials Science and Engineering*, vol. 1107, p. 012116 (2021)
31. B. Callegari, T.N. Lima, R.S. Coelho, The influence of alloying elements on the microstructure and properties of Al–Si–based casting alloys: a review. Metals (Basel) **13**, 1174 (2023)
32. J. Sun et al., Microstructure and tensile properties of a cast eutectic Al–Si–Cu alloy modified by Zr and V. Met. Mater. Int. **27**, 5436–5449 (2021)
33. Y.-C. Tzeng, J.-K. Nieh, H.-Y. Bor, S.-L. Lee, Effect of trace Be and Sc additions on the mechanical properties of A357 alloys. Metals (Basel) **8**, 194 (2018)
34. J.G. Kaufman, E.L. Rooy, *Aluminum Alloy Castings: Properties, Processes, and Applications* (ASM International, Almere, 2004)
35. W.R. Osório, N. Cheung, J.E. Spinelli, P.R. Goulart, A. Garcia, The effects of a eutectic modifier on microstructure and surface corrosion behavior of Al–Si hypoeutectic alloys. J. Solid State Electrochem. **11**, 1421–1427 (2007)
36. Q.G. Wang et al., Size effects in aluminium alloy castings. Acta Mater. **58**, 3006–3013 (2010)
37. M. Zhu, Z. Jian, G. Yang, Y. Zhou, Effects of T6 heat treatment on the microstructure, tensile properties, and fracture behavior of the modified A356 alloys. Mater. Des. **1980–2015**(36), 243–249 (2012)
38. E.A. Elsharkawi, A.M. Samuel, F.H. Samuel, E. Simielli, G.K. Sigworth, Influence of solutionizing time, modification, and cooling rate on the decomposition of Mg-containing iron intermetallic phase in 357 alloys. in *Transactions of the American Foundry Society*, pp. 55–65 (2012)
39. R. Mahmudi, P. Sepehrband, H.M. Ghasemi, Improved properties of A319 aluminum casting alloy modified with Zr. Mater. Lett. **60**, 2606–2610 (2006)
40. J. Rakhmonov, G. Timelli, F. Bonollo, Characterization of the solidification path and microstructure of secondary Al-7Si-3Cu-0.3 Mg alloy with Zr V and Ni additions. Mater Charact **128**, 100–108 (2017)
41. T. Tunçay, D. Özyürek, D. Dişpinar, S. Tekeli, The effects of Cr and Zr additives on the microstructure and mechanical properties of A356 alloy. Trans. Indian Inst. Met. **73**, 1273–1285 (2020)
42. L. Ji et al., Effect of erbium–zirconium composite modifications on the microstructure and mechanical properties of A356 aluminum alloy. in *High Performance Structural Materials: Proceedings of Chinese Materials Conference 2017 18th* 87–94 (Springer, 2018)
43. W. Liu, W. Xiao, C. Xu, M. Liu, C. Ma, Synergistic effects of Gd and Zr on grain refinement and eutectic Si modification of Al-Si cast alloy. Mater. Sci. Eng. A **693**, 93–100 (2017)
44. T. Gao et al., Structural and morphological evolution of Fe–rich phases in Al–xMg–6Si–4Fe alloys. Results Mater. **3**, 100036 (2019)
45. E.A. Elsharkawi, M.H. Abdelaziz, H.W. Doty, S. Valtierra, F.H. Samuel, Effect of β-Al_5FeSi and π-$Al_8Mg_3FeSi_6$ phases on the impact toughness and fractography of Al–Si–Mg-based alloys. Int. J. Metalcast. **12**, 148–163 (2018). https://doi.org/10.1007/s40962-017-0153-8

46. J.Q. Guo, K. Ohtera, An intermediate phase appearing in Ll_2-Al_3Zr to DO23-Al_3Zr phase transformation of rapidly solidified Al-Zr alloys. Mater. Lett. **27**, 343–347 (1996)
47. M. Tash, F.H. Samuel, F. Mucciardi, H.W. Doty, Effect of metallurgical parameters on the hardness and microstructural characterization of as-cast and heat-treated 356 and 319 aluminum alloys. Mater. Sci. Eng. A **443**, 185–201 (2007)
48. Q. Chen et al., Effect of T6 heat treatment on microstructure and mechanical properties of large-weight aluminum alloy flywheel housing parts formed by local-loading squeeze casting. J. Market. Res. **24**, 1612–1625 (2023)
49. S.S. Dash, D. Chen, A review on processing–microstructure–property relationships of Al–Si alloys: recent advances in deformation behavior. Metals (Basel) **13**, 609 (2023)
50. H.A. Elhadari, H.A. Patel, D.L. Chen, W. Kasprzak, Tensile and fatigue properties of a cast aluminum alloy with Ti, Zr and V additions. Mater. Sci. Eng. A **528**, 8128–8138 (2011)
51. A. De Mori, G. Timelli, A. Fabrizi, F. Berto, Influence of Cu content on the microstructure and high-temperature tensile and fatigue properties of secondary $AlSi_7Mg_{0.3}VZr$ alloys. Mater. Sci. Eng. A **816**, 141310 (2021)